https://doi.org/10.5194/egusphere-2024-796
Preprint. Discussion started: 25 March 2024

Countering the effect of ocean acidification in coastal sediments through carbonate mineral additions

Kadir Bice[1,*], Tristen Myers[2,#], George Waldbusser[2], Christof Meile[1,*]

[1] Department of Marine Sciences, University of Georgia, Athens GA 30602

[2] Ocean Ecology and Biogeochemistry, College of Earth, Ocean, and Atmospheric Sciences, Oregon State University, Corvallis, OR 97331

[#] now at: Pacific Northwest National Laboratory, Sequim, WA 98382

Correspondence to: Kadir Bice (bicekadir@gmail.com), Christof Meile (cmeile@uga.edu)

Abstract. Along with its impact on calcifying plankton, ocean acidification also affects benthic biogeochemistry and organisms. Compared to the overlying water, fluid composition in sediments is altered through the effect of the mineralization of organic matter, which can further lower both pH and the carbonate saturation state. This can potentially be counteracted by the addition of carbonate minerals to the sediment surface. To explore the biogeochemical effects of mineral additions to coastal sediments, we experimentally quantified carbonate mineral dissolution kinetics, and then integrated this data into a reactive transport model that represents early diagenetic cycling of C, O, N, S and Fe, and traces total alkalinity, pH and saturation state of $CaCO_3$. Model simulations were carried out to delineate the impact of mineral type and amount added, porewater mixing and organic matter mineralization rates on sediment alkalinity and its flux to the overlying water. Model results showed that the added minerals undergo initial rapid dissolution and generate saturated conditions. Aragonite dissolution led to higher alkalinity concentrations than calcite. Simulations of carbonate mineral additions to sediment environments with low rates of organic matter mineralization exhibited a significant increase in mineral saturation state compared to sediments with high CO_2 production rates, highlighting the environment-specific extent of the buffering effect. Our work indicates that carbonate additions have the potential to effectively buffer surficial sediments over multiple years, yielding biogeochemical conditions that counteract the detrimental effect of OA conditions on larval recruitment, and potentially increase benthic alkalinity fluxes to support marine carbon dioxide removal (mCDR) in the overlying water.

1. Introduction

The ocean absorbs large amounts of anthropogenic CO_2 due to the transformation of dissolved CO_2 into predominantly bicarbonate. While lowering the rate of atmospheric CO_2 increase, this uptake causes ocean acidification (OA), lowering pH

https://doi.org/10.5194/egusphere-2024-796
Preprint. Discussion started: 25 March 2024

and mineral saturation states in the ocean (Doney et al., 2009). The effect of CO_2 additions depends on the buffering capacity of the water. This is quantified by its alkalinity (Middelburg et al., 2020), which in the ocean largely reflects the balance and magnitude of formation/dissolution of calcium carbonate, primary production, and respiration (Fry et al., 2015). Respiration decreases and $CaCO_3$ dissolution produces total alkalinity (TA; Dickson 1981) and increases pH (Su et al., 2020; Green et al., 2009; Andersson et al., 2005).

In coastal systems, ocean-freshwater mixing, terrestrial inputs, and active biogeochemical transformations (Cai et al., 2017; Soetaert et al., 2007) lead to natural fluctuations in pH that are large and decoupled from the decrease in pH observed in the open ocean (Hofmann et al., 2011). Especially in shallow water environments, sediments play a significant role as benthic fluxes can constitute a substantial alkalinity source to the overlying water, increasing its buffering capacity against ocean acidification (Rassmann et al., 2016; Krumins et al., 2013; Cyronak et al., 2013b). Sediments receive organic matter (OM) from the overlying water which fuels the dissolution of carbonate minerals and early diagenetic processes. Aerobic respiration can lead to steep pH decreases within the oxygenated sediment and the interaction of OM mineralization and mineral dissolution determines the balance of the porewater carbonate system (Burdige et al., 2010; Jourabchi et al., 2005). Mineral dissolution and early diagenesis are connected through the changes in carbonate system which impacts mineral saturation states and hence the rate of dissolution (e.g., Morse et al., 2007). Apart from its impact on mineral dissolution, OM mineralization is also a significant contributor to alkalinity generation, in particular under suboxic and anoxic conditions (Gimenez et al., 2018). These early diagenetic processes determine the composition of the porewaters, which affect benthic calcifying organisms; furthermore, they can affect the biogeochemical conditions in the overlying water through benthic fluxes releasing nutrients and alkalinity.

Biological production of minerals by shell formation depends on the saturation state of the water, food availability, and other environmental parameters (Waldbusser et al., 2015). By altering saturation state, OA impacts ocean life, especially calcifying organisms in their larval and juvenile stages, eventually deteriorating coastal communities, fisheries, and shellfish industry (Fabry et al., 2008; Ekstrom et al., 2015; Barton et al., 2015). In shallow waters, strong benthic-pelagic coupling may impact organisms in multiple growth stages by changing carbonate conditions in both water and sediment columns (Waldbusser & Salisbury, 2014). However, in sediments, this impact is more critical due to porewater pH generally being lower than in the overlying water, in particular when sediment O_2 uptake is elevated due to biological transport by deposit feeders (Aller, 1982), or more broadly, burrowing and irrigation activities by benthic macrofauna. This exposes benthic organisms that live in the upper layers of the sediment, for example because they have shorter siphons to access to the overlying water, to more corrosive conditions (Green et al., 2013; Waldbusser & Salisbury, 2014; Zwarts & Wanink et al., 1989). Enhanced supply of O_2 into the sediment lowers pH, which can increase carbonate dissolution and lead to elevated flux of alkalinity and DIC to the water column (Mucci et al., 2000; Burdige et al., 2007). This extends the impact of the benthos to the overlying water and affects the impact of ocean acidification in shallow water environments.

https://doi.org/10.5194/egusphere-2024-796
Preprint. Discussion started: 25 March 2024

In this study, we investigate the effects of the addition of carbonate minerals in the coastal sediments focusing on benthic alkalinity generation and release in a shallow water environment. Such ocean alkalinity enhancement (OAE) aims to buffer increased dissolved CO_2 in the ocean by dissolving carbonate or silicate minerals, producing alkalinity. OAE is mainly studied for its effect on ocean - atmosphere CO_2 exchange (Renforth & Henderson, 2017) and its potential to mitigate ocean acidification and lower atmospheric CO_2 concentrations (carbon dioxide removal; CDR). Previous studies have shown that OAE has the potential to reverse global ocean acidification in an intermediate CO_2 emission scenario (RCP 4.5) and reduce its impacts if emissions were to continue to rise throughout the 21st century (RCP 8.5) (Taylor et al., 2016). To date, OAE implementations are mostly undertaken in the open ocean and are aimed at identifying the potential of scaling up the CDR efforts to a global scale (Montserrat et al., 2017). Recent studies also focused on the impact of OAE on marine ecosystems such as fish and plankton communities (Goldenberg et al., 2024; Paul et al., 2024). Only a few studies focused on coastal OAE and even fewer on sedimentary applications (Green et al., 2009, 2013; Hangx et al., 2009), where the effectiveness of OAE mainly depends on the dissolution rate of the mineral which is controlled by the mineral and the chemistry of the water and physical properties of the environment (Hartmann et al., 2013; Montserrat et al., 2017). One benefit of implementing OAE in coastal sediments is the generally higher rate of organic matter remineralization. This elevated CO_2 generation aids mineral dissolution, given most overlying marine waters are typically super-saturated with respect to carbonate minerals. Here, we simulate this effect of adding carbonate minerals to the sediment using a reactive transport model. We use measurements of carbonate mineral dissolution rates to assess the extent and duration of buffering in surficial sediments, and the impact on benthic alkalinity fluxes. Building on the previous work by Krumins et al. (2013) and Rassman et al. (2016) that explored the interaction of carbonate chemistry with early diagenesis in coastal sediments, our work identifies factors that determine the impact of sediment alkalinization on the spatial and temporal distribution of buffering by exploring the effect of mineral type, amount, organic matter remineralization rate and bioturbation.

2. Methods

2.1. Dissolution experiments

Dissolution rates for the minerals used in this model were derived from lab-based experiments detailed in Myers (2022). We provide pertinent details below. Two biomineral calcium carbonates, calcitic oyster shells *Crassostrea gigas* (below referred to as "bio-calcite") and aragonitic clam soft-shell clam shells, *Mya arenaria*, ("bio-aragonite") were collected from Oregon Oyster Farm in Newport, Oregon, USA and from Broad Cove in Yarmouth, Maine, USA, respectively. The biomineral samples were briefly cleaned, dried, crushed and sieved through a 2000 μm sieve and retained on 710 μm, for an approximately median grain size of 1 mm. We measured the mineral dissolution rate across four saturation states experimentally; $\Omega_{calcite}$ = 0.25 (low), 0.45 (mid), 0.85 (hi) and 1.03 (saturated); carbonate chemistry conditions are detailed in Table S1. A flow-through, feedback-controlled with pH monitoring and CO_2 injection seawater system similar to Waldbusser et al. (2011) was used for manipulations at the Hatfield Marine Science Center (HMSC), Newport, OR, USA (additional details in Myers, 2022). pH measurements from each manipulation tank were compared against a benchtop meter

https://doi.org/10.5194/egusphere-2024-796
Preprint. Discussion started: 25 March 2024

daily during the experiment. pH was additionally compared against a reference sample in which pCO_2 and TCO_2, in situ temperature and salinity were measured to calculate pH on the NBS scale. pH (all tanks) and temperature (low and pre-treatment tanks) data were recorded every ten minutes. The correlation coefficient between measured benchtop pH data and the pH data calculated from pCO_2/TCO_2 measurements for header tanks in all experiments was consistently greater than 0.9 across all experiments. Plug-flow style dissolution chambers were 2.5 cm ID, 12.7 cm long, schedule 40 PVC pipe, with 150 µm Nitex mesh on either end of the upright chambers. Approximately 50 (± 0.1) grams of biomineral were used in each chamber, water was initially added slowly and agitated to remove air bubbles prior to initiating flow. Flowrates were controlled to 17 (± 1.2) mL min^{-1} and experiments were run for three to four days to verify consistent alkalinity concentrations, as observed in trials conducted to optimize the experiment (Myers, 2022). Using the inlet and outlet measured alkalinity concentrations from an individual chamber (mmol alkalinity L^{-1}), the measured flow rate (mL min^{-1}), and the known amount of sample added ($g_{mineral}$), the change in alkalinity in mmol alkalinity $g_{mineral}^{-1}$ d^{-1} was recorded as (Eq. 1):

$$\Delta = \frac{([alkalinity]_{outlet} - [alkalinity]_{inlet})}{(mineral\ amount * flow\ rate)} \quad (1)$$

The early diagenetic model (see below) uses a rate law in which the volumetric dissolution rate R_d (in $mol_{mineral}$ $m^{-3}_{sediment}$ d^{-1}) depends on the concentration of the mineral ($mol_{mineral}$ $m^{-3}_{sediment}$), the saturation state Ω (= ion concentration product/solubility K_{sp}) and the dissolution rate constant k_d (d^{-1}) (Jourabchi et al., 2008):

$$R_d = k_d[Mineral](1 - \Omega)^n \quad (2)$$

In the experiment, the dissolving mineral is the entire solid phase, so that $g_{mineral}$ = $g_{solid\ phase}$. Hence, the mineral concentration in $mol_{mineral}/g_{solid\ phase}$ is the molecular weight of the mineral ($MW_{mineral}$) and k_d can be calculated as:

$$k_d = \frac{\Delta * MW_{mineral}}{\frac{dTA}{dR} * (1 - \Omega)^n} \quad (3)$$

where *dTA/dR* is the mineral to alkalinity stoichiometric ratio in the dissolution reaction (+2; Table 3) and *n* is the rate order.

2.2. Carbonate Chemistry Measurements

Alkalinity

Open-cell alkalinity titrations were conducted over the course of the experiment, utilizing a two-point titration after Edmond (1970), as modified by Waldbusser (2011). A micrometer burette was used with a micro pH probe with precisions of 0.002 mL and ± 0.02, respectively. The probe was calibrated with NBS calibration standards (pH = 4, 7, and 10) daily before being used to take measurements. As outlined in Waldbusser et al. (2011), Baker Analyzed Reagent grade 0.0995-0.1005 normal HCl acid was used as the titrant with reagent grade NaCl to a final molar concentration of 0.7 to minimize gap junction potentials during titrations. Analytical precision and accuracy were compared against triplicate titrations and Dickson CRM batch 142, respectively, and found to have an average coefficient of variance of 0.07% and typically ±16 µmol or less, for precision and accuracy.

https://doi.org/10.5194/egusphere-2024-796
Preprint. Discussion started: 25 March 2024

Dissolved Inorganic Carbon, pCO_2, and Carbonate Calculations

Validation samples for pCO_2/TCO_2 samples were collected in clean amber glass ~350 ml bottles preserved with 30 microliters of saturated $HgCl_2$ and sealed with polyurethane-lined crimp-sealed metal caps. Analysis via the Burkalator was carried out to measure pCO_2 and TCO_2 via near-infrared detection following the procedure of Bandstra et al. (2006), modified for discrete samples as in Hales et al. (2005), Barton et al. (2012), and Hales et al. (2017). Liquid and gas standards were employed to ensure the accuracy of pCO_2/TCO_2 measurements. The system can resolve the accuracy and precision of TCO_2 concentrations within ± 0.02% and 2% for pCO_2 (Hales et al., 2017). Carbonate chemistry parameters were calculated using dissociation constants from Millero (2010). Salinity was measured on the sample bottles following pCO_2/TCO_2 measurements via a salinometer (8400B "Autosal" Laboratory Salinometer; Guildline Instruments, Sorrento, FL, US).

2.3. Reactive transport modeling

A one-dimensional diagenetic model was developed to simulate the distribution of chemical species with depth in the sediment over time. The model domain extended 20 cm deep into the sediment discretized into 50 intervals with a linearly increasing grid size of 1 mm at the top and 1 cm at the bottom. The model included 13 state variables, representing chemicals involved in the main early diagenetic reactions, and mineral dissolution/precipitation (Table 1). At the upper boundary, the concentrations of solutes and fluxes of solids were imposed, while at the bottom boundary, no gradient conditions were imposed for all chemicals.

Table 1: State variables and their upper boundary conditions. Concentrations as a function of salinity are computed with *aquaenv* (Hofmann et al. 2010) for a given pressure and temperature.

Variable	Notation	Boundary condition
Oxygen	O_2	0.2 mM
Sulfate	SO_4^{2-}	Seawater composition, f(salinity)
Total sulfide	TS	0 mM
Dissolved inorganic carbon	DIC	equilibrium with a given alkalinity and pH 7.96
Total alkalinity	TA	1.9 mEq/L (measured at Yaquina Bay)
Calcium	Ca^{2+}	Seawater composition, f(salinity)
Magnesium	Mg^{2+}	Seawater composition, f(salinity)
Iron	Fe^{2+}	0 mM
Ammonium	NH_4^+	0 mM
Nitrate	NO_3^-	0.02 mM
Carbonate mineral (s)	$CaCO_3$	F = 0 µmol cm^{-2} yr^{-1}

https://doi.org/10.5194/egusphere-2024-796
Preprint. Discussion started: 25 March 2024

Iron oxides (s)	$Fe(OH)_3$	F = 1 µmol cm^{-2} yr^{-1}
Iron sulfide (s)	FeS	F = 0 µmol cm^{-2} yr^{-1}

The spatio-temporal evolution of the concentrations was described by an advection-diffusion equation with the addition of bioturbation and bioirrigation and the effect of reactions. Bioturbation was treated as a diffusive process (Boudreau, 1997) and bioirrigation was described as a non-local exchange between porewater at depth and the overlying water (Boudreau, 1984). The governing equations were:

$$\phi \frac{\partial C_i}{\partial t} = -\frac{\partial \phi u C_i}{\partial x} + \frac{\partial}{\partial x}\left(\phi (D_i + D_b)\frac{\partial C_i}{\partial x}\right) + \sum_r s_{ir} R_r + B_i \quad (4)$$

$$(1-\phi)\frac{\partial C_j}{\partial t} = -\frac{\partial (1-\phi) v C_j}{\partial x} + \frac{\partial}{\partial x}\left((1-\phi) D_b \frac{\partial C_j}{\partial x}\right) + \sum_r s_{jr} R_r \quad (5)$$

where t is time, x is depth in sediment, ϕ is porosity, C_i (C_j) is the concentration of the solute i (in mol/volume pore fluid; solid j in mol/volume solid phase), u is the burial velocity for solutes (v for solids), D_i is the diffusion coefficient of the solute i, D_b is the depth bioturbation coefficient, R_r is the rate of production/consumption through reaction r (in mass/total volume and time); B_i represents bioirrigation.

Porosity is constant with time but depth-dependent and exponentially decreases with depth reflecting steady state sediment compaction (Eqn. 6):

$$\phi_x = \phi_\infty + (\phi_0 - \phi_\infty) e^{-\frac{x}{\gamma}} \quad (6)$$

where ϕ_∞ and ϕ_0 are the porosities at infinite depth and at the top of the sediment, respectively, and γ is the e-folding distance for the porosity. Burial velocities were corrected for compaction (Berner, 1980):

$$u_x = v_\infty \frac{\phi_\infty}{\phi} \quad (7)$$

$$v_x = v_\infty \frac{(1-\phi_\infty)}{(1-\phi)} \quad (8)$$

Diffusion coefficients were calculated using the R package *marelac* after Boudreau (1997) at a given salinity, temperature and pressure (Soetaert et al., 2010) and corrected for tortuosity (Boudreau, 1996) so that:

$$D_i = \frac{D_{aq,i}}{1 - 2ln(\phi_x)} \quad (9)$$

where D_{aq} is the molecular diffusion coefficient of solute i in solution. The bioturbation coefficient decreases exponentially with depth below the mixed layer,

$$D_b = D_{b0} e^{-\max(0,\ x - x_m)} \quad (10)$$

where x_m is the depth of mixed layer and D_{b0} is the bioturbation coefficient at the SWI, calculated as a function of water depth (Middelburg, 1997).

https://doi.org/10.5194/egusphere-2024-796
Preprint. Discussion started: 25 March 2024

Bioirrigation is defined as an exchange between the surface layer and deeper layers of the sediment which was constrained by an exponentially decreasing bioirrigation coefficient:

$$B_x = \alpha_0 e^{(-\frac{x}{\varepsilon})} \phi_x (C_{i,0} - C_{i,x}) \quad (11)$$

where α_0 is the bioirrigation coefficient at the SWI, ε is the e-folding distance for bioirrigation and $C_{i,x}$ is the concentration of solute i at depth x.

Table 2: Environmental parameters

Parameter	Value
Salinity	35
Temperature	12 deg C
Overlying water pH	7.96
Pressure	1.013 bar
Seawater density	1.027 kg L^{-1}
Sediment density	2.65 g cm^{-3} (Boudreau, 1997)
Porosity decay with depth ($\boldsymbol{\gamma}$)	5 cm (Rooze et al., 2016)
Porosity at the surface ($\boldsymbol{\phi_0}$)	0.8
Porosity at infinite depth ($\boldsymbol{\phi_\infty}$)	0.6
Sedimentation at infinite depth ($\boldsymbol{v_\infty}$)	0.5 cm yr^{-1} (Middelburg, 1997)
Bioturbation mixing coefficient at the top ($\boldsymbol{D_{b0}}$)	30 cm^2 yr^{-1} (Middelburg, 1997)
Bioturbation e-folding distance	1 cm (Soetaert et al., 1996)
Depth of mixed layer ($\boldsymbol{x_m}$)	4 cm (Rooze et al., 2016)
Bioirrigation rate constant at the top ($\boldsymbol{\alpha_0}$)	200 yr^{-1} (Wang & Capellen, 1996; Meile & Capellen, 2003)
Bioirrigation decay with depth ($\boldsymbol{\varepsilon}$)	3.5 cm (Thullner et al., 2009)

Reactions considered in the model include organic matter mineralization with aerobic and anaerobic pathways, reoxidation of reduced species and mineral formation/dissolution reactions (Table 3). Each reaction has an impact on the total alkalinity (TA), which is defined as (Wolf-Gladrow et al., 2007):

$$TA = [HCO_3^-] + 2[CO_3^{2-}] + [B(OH)_4^-] + [OH^-] + [HPO_4^{2-}] + 2[PO_4^{3-}] + [H_3SiO_4^-] + [NH_3] + [HS^-] - [H^+] - [HSO_4^-] - [HF] - [H_3PO_4] - [HNO_2] \pm other\ bases/acids \ldots$$

Organic matter is mineralized using O_2, NO_3^-, iron (oxyhydr)oxides (FeOx) and SO_4^{2-} as terminal electron acceptors and modeled with Monod kinetics. The OM mineralization rate was adjusted to yield a TA flux of ~1200 µmol cm^{-2} yr^{-1}. This value was chosen to match open core top incubations measured in Yaquina Bay (Myers, 2022), and resulting R_C^0 value was comparable to earlier measurements by D'Andrea & DeWitt (2009), but higher than values reported for deeper coastal shelf

https://doi.org/10.5194/egusphere-2024-796
Preprint. Discussion started: 25 March 2024

environments (Wang & Van Capellen, 1996; Krumins et al., 2013). Reactions considered further include nitrification, iron oxidation, sulfide oxidation with O_2 and FeOx, and iron sulfide oxidation, as well as the formation/dissolution of $CaCO_3$ minerals and FeS (Table 3). Following Rooze et al. (2020), at each time step, DIC is speciated to calculate CO_3^{2-} concentration and pH from DIC and alkalinity, assuming seawater concentrations of borate and negligible contributions of
190 phosphate, silicic acid, nitrite and hydrogen fluoride and other acids or bases.

Table 3: Reactions included in the model. Benthic primary production is assumed to be negligible and organic matter has Redfield stoichiometry (a = 1, b = 16/106, c = 1/106). Alkalinity production or consumption in each reaction is determined following Wolf-Gladrow et al. (2007). The total mineralization rate is defined as $R_C = R_C^0 * \exp(-x/\gamma_{om})$ after Wang & Cappellen (1996)

Reaction	**dTA/dR**	**Reaction rate**
Organic Matter Mineralization		
$(CH_2O)_a(NH_3)_b(H_3PO_4)_c$ + a O_2 => a CO_2 + b NH_4^+ + c HPO_4^{2-} + (-b+2c) H^+ + a H_2O	b - c	$R_{O_2}^m = RC\ [O_2] / (K_{O_2}^m + [O_2])$
$(CH_2O)_a(NH_3)_b(H_3PO_4)_c$ + 4a/5 NO_3^- + (4a/5 +b -2c) H^+ => a CO_2 + b NH_4^+ + c HPO_4^{2-} + 2a/5 N_2 + 7a/5 H_2O	4a/5 + b - c	$R_{NO_3}^m = \left(RC - R_{O_2}^m\right)[NO_3] / (K_{NO_3}^m + [NO_3])$
$(CH_2O)_a(NH_3)_b(H_3PO_4)_c$ + 4a $Fe(OH)_3$ + (8a+b-2c) H^+ => a CO_2 + b NH_4^+ + c HPO_4^{2-} + 4a Fe^{2+} + 11a H_2O	b - c + 2*4a	$R_{FeOx}^m = \left(RC - R_{O_2}^m - R_{NO_3}^m\right)[FeOx] / (K_{FeOx}^m + [FeOx])$
$(CH_2O)_a(NH_3)_b(H_3PO_4)_c$ + a/2 SO_4^{2-} + (a/2 +b -2c) H^+ => a CO_2 + b NH_4^+ + c HPO_4^{2-} + a/2 HS^- + a H_2O	b - c + a	$R_{SO_4}^m = \left(RC - RC_{O_2}^m - R_{NO_3}^m - R_{FeOx}^m\right)[SO_4] / (K_{SO_4}^m + [SO_4])$
Secondary reactions		
NH_4^+ + 2O_2 => NO_3^- + 2H^+ + H_2O	-2	$R_{NH_4}^o = k_{NH_4}^o [NH_4][O_2]$
Fe^{2+} + 5/2 H_2O + 1/4 O_2 => $Fe(OH)_3$ + 2H^+	-2	$R_{Fe}^o = k_{Fe}^o [Fe^{2+}][O_2]$

https://doi.org/10.5194/egusphere-2024-796
Preprint. Discussion started: 25 March 2024

$HS^- + 2O_2 => SO_4^{2-} + H^+$	-2	$R^o_{TS} = k^o_{TS}[TS][O_2]$
$HS^- + 8Fe(OH)_3 + 15H^+ => SO_4^{2-} + 8Fe^{2+} + 20H_2O$	+14	$R^{of}_{TS} = k^{of}_{TS}[TS][FeOx]$
$FeS + 2O_2 => Fe^{2+} + SO_4^{2-}$	0	$R^o_{FeS} = k^o_{FeS}[FeS][O_2]$
Mineral precipitation/dissolution		
$FeS + 2H^+ <=> Fe^{2+} + 2HS^-$	+2 (dis)/-2 (prec)	$\Omega_{FeS} = [Fe][TS]/([H^+]K^{sp}_{FeS}\rho^2_{sw})$ $R_{FeS} = \begin{cases} k^f_{FeS}(\Omega_{FeS} - 1), & \text{if } \Omega_{FeS} \geq 1 \\ k^d_{FeS}[FeS](1 - \Omega_{FeS}), & if\ \Omega_{fes} < 1 \end{cases}$
$CaCO_3 <=> Ca^{2+} + CO_3^{2-}$	+2 (dis)/-2 (prec)	$\Omega_M = [Ca^{2+}][CO_3]/(K^{sp}_M \rho^2_{sw})$ $R_M = \begin{cases} k^f_M(\Omega_M - 1), \text{if } \Omega_M \geq 1 \\ k^d_M[Mineral](1 - \Omega_M)^n, if\ \Omega_M < 1 \end{cases}$

Table 4: Reaction constants. Carbonate dissolution rate constants determined experimentally in this study are described in the results.

Reaction parameters	Value	Source
R^0_C	400 µmol C cm^{-3} yr^{-1}	Experimental
γ_{om}	5 cm	(Wang & Capellen, 1996)
$K^m_{O_2}$	0.02 mM	(Rooze et al., 2016)
$K^m_{NO_3}$	0.004 mM	(Rooze et al., 2016)
K^m_{FeOx}	130 mM	(Rooze et al., 2016)
$K^m_{SO_4}$	1.6 mM	(Rooze et al., 2016)
$k^o_{NH_4}$	5000 mM^{-1} yr^{-1}	(Rooze et al., 2016)
k^o_{Fe}	140 000 mM^{-1} yr^{-1}	(Rooze et al., 2016)
k^o_{TS}	160 mM^{-1} yr^{-1}	(Rooze et al., 2016)
k^{of}_{TS}	6 mM^{-1} yr^{-1}	(Rooze et al., 2016)
k^o_{FeS}	300 mM^{-1} yr^{-1}	(Rooze et al., 2016)
K^{sp}_{FeS}	$10^{-2.2}$ $(mol/kg)^2$	Wang & Van Capellen (1996)
k^f_{FeS}	$6*10^{-6}$ mol g^{-1} yr^{-1}	Wang & Van Capellen (1996)
k^d_{FeS}	10^{-3} yr^{-1}	Wang & Van Capellen (1996)
$K^{sp}_{calcite}$	$4.31*10^{-7}$ $(mol/kg)^2$	f(salinity) (Mucci et al., 1983)

https://doi.org/10.5194/egusphere-2024-796
Preprint. Discussion started: 25 March 2024

$K^{sp}_{aragonite}$	6.82*10^{-7} (mol/kg)^2	f(salinity) (Mucci et al., 1983)

Application

To establish initial conditions, each simulation was first run to steady state before adding 8 or 16 weight % (weight of mineral/ total weight of the sediment) $CaCO_3$ to the top 2 cm of sediment, respectively. The spin-up simulations were specific to each model run, and as such represent the environmental conditions (e.g., high vs. low rate of mineralization, or a setting in which either aragonite or calcite are the only carbonate mineral considered). Then, a 2-year transient simulation was run to assess the impact of the alkalinization experiment. To investigate the temporal evolution of buffering over longer time frames, additional 50-year simulations were carried out. To assess the potential impact of adding minerals to the sediment, effectively diluting the concentration of organic matter in the surficial sediment, we also carried out simulations in which the model was modified to include particulate organic matter (POM) and using an OM mineralization rate dependent on POC concentration (see Supplementary Information).

We tested the impact of several environmental factors on the buffering effect of carbonate mineral additions to surficial sediments in comparison to the baseline addition scenario (i.e., 8% calcite addition). Specifically, we varied the rate of OM mineralization, as terminal metabolism has a major impact on sediment redox conditions, porewater composition and relative importance of different metabolic pathways; R_C^0 was varied from the baseline value of 400 to 200 µmol/cm^3/yr to represent environments with different O_2 penetration depths and differing mineralization rates. We also varied the deposition flux of iron (oxy)hydroxides from 1 to 10 µmol/cm^2/yr to assess differences between sites that vary in the extent of coupling between Fe, S and C cycles. Finally, the depth of the bioturbated layer affects the distribution of minerals added, which may impact the effectiveness of the extent of buffering; it was varied from surficial mixing in baseline implementation (i.e., 4 cm) to the global average depth of bioturbation of 10 cm (Boudreau, 1997).

CO_2 drawdown

We estimated the potential impact of enhanced sediment TA fluxes on atmospheric CO_2 uptake in an enclosed bay using a simple box model. Water exchange is due to the tides, but riverine input is neglected, capturing summertime conditions at Yaquina Bay, OR (USA) when river discharge is low and metabolic rates are elevated. As described in detail in the Supplementary Information, we first estimated tidal water exchange from water level measurements, and used unpublished temperature, salinity, and pH data (pers. comm. G. Waldbusser) from Yaquina Bay to constrain the characteristics of the inflowing marine (alkalinity = 2.2 mmol L^{-1}, pH = 8.0) and outflowing bay water (alkalinity = 1.9 mmol L^{-1}, pH = 7.96) at a proximal sample site. Combined with our modeled benthic exchange fluxes, this allowed us to estimate the alkalinity production in the water column which we interpret to be the consequence of net photosynthesis and aerobic respiration. Next, we used the alkalinity and pH to calculate the DIC and converted the net alkalinity production rate into net DIC production in the water column, assuming Redfield stoichiometry. This finally allowed us to estimate the CO_2 exchange flux necessary to close the DIC mass balance for benthic fluxes with and without mineral additions to quantify its effect on ocean CO_2 uptake.

https://doi.org/10.5194/egusphere-2024-796
Preprint. Discussion started: 25 March 2024

3. Results & Discussion

3.1. Mineral Dissolution Rates

Dissolution rates of minerals were highest under highly undersaturated conditions (Figure 1). For a given mineral saturation state, bio-aragonite dissolved slightly faster than bio-calcite. Dissolution rates are approximately proportional to the degree of saturation. This relationship is in line with previous reactive transport models focused on mineral dissolution (Morse et al., 2007; Jourabchi et al., 2005; 2008; Krumins et al., 2013). Thus, the dissolution rate constant k_d for each mineral was estimated using Eqns. (1) and (2) with a dissolution order (n) of 1. Kinetic constant for aragonite dissolution was previously reported as 5 yr^{-1} (Luff & Wallmann, 2003) which was comparable to the 5.2 yr^{-1} derived from our measurements. For n =1, Jourabchi et al. (2005), reported a dissolution rate constant of 3.65 yr^{-1} while our estimation for bio-calcite was 5 yr^{-1}.

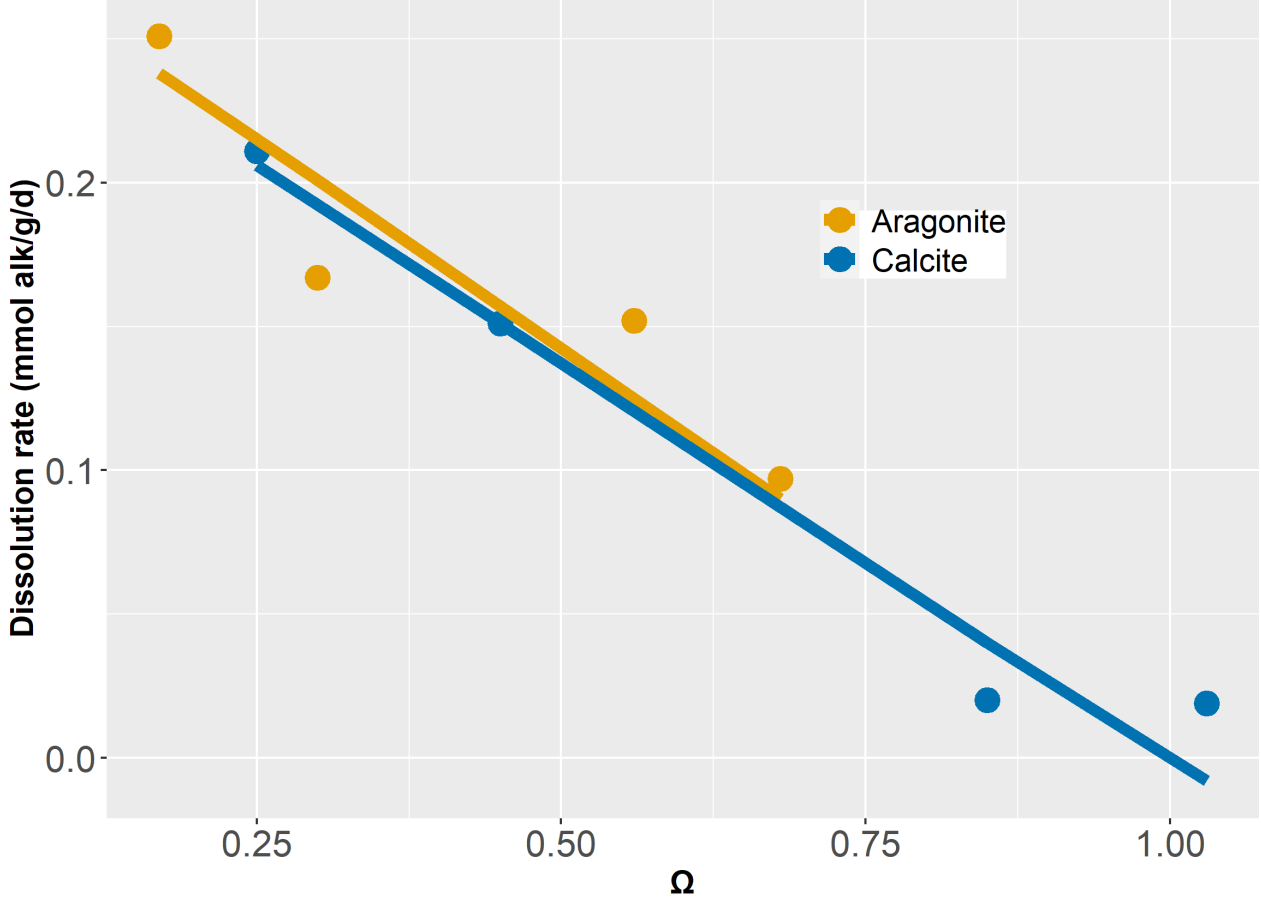

Figure 1: Saturation state for aragonite and calcite vs. their respective dissolution rates (mmol alk/g_{solid}/d). Lines show the fit with n=1.

https://doi.org/10.5194/egusphere-2024-796
Preprint. Discussion started: 25 March 2024

3.2. Early Diagenetic Modeling

To assess the impact of sediment alkalinization through the addition of carbonate minerals to the sediment, early diagenetic model simulations were carried out that describe the spatio-temporal distribution of porewater and solid phase constituents. Prior to the addition of minerals, the simulated porewater profiles show sequential depletion of electron acceptors with depth, with O_2, NO_3^- and reactive FeOx only present in the top 5 cm (solid lines in Figure 2). SO_4^{2-} is present throughout the depth range and only decreases by about 2.5 mM. As a result of mineralization reactions, the concentrations of reduced porewater constituents (TS, NH_4^+, Fe^{2+}) increase with depth (Figure 2). Reduced dissolved iron (Fe^{2+}) peaked around 1 cm then decreased with depth due to the precipitation of FeS, which in our baseline simulation limited the build-up of TS and Fe^{2+}. These porewater profiles reflect the sequential use of electron acceptors in the mineralization of organic matter, through aerobic respiration and anaerobic pathways such as denitrification, dissimilatory iron and sulfate reduction. The dominant OM mineralization pathway was SO_4^{2-} reduction (78.9%) followed by aerobic mineralization (17.2%), denitrification (3.9%) and iron reduction (0.06%).

DIC and TA show pronounced concentration increases with depth, reflecting OM mineralization (Figure 2 i,j). The pH profile exhibits a rapid decrease in the top centimeter to about 7, showing the impact of CO_2 production without the concurrent consumption of protons through aerobic mineralization (Table 3; Jahnke et al., 1994; Green et al., 2013). Below the oxic layer, active anaerobic OM mineralization pathways such as iron and sulfate reduction can generate considerable amounts of TA if the reaction products are not oxidized (Thomas et al., 2009). This was observed in the buildup of reduced species such as TS (discussed below) which limited the drop in pH and increased saturation state (from 0.5 to > 0.8) in the deeper layers of the sediment (Fig. 2 k,l). pH values were in the lower part of the range reported in Krumins et al. (2013), reflecting the lack of carbonates buffering the pH prior to the mineral additions. Sulfate reduction produced the majority of the TA and DIC (Figure 3), consistent with the findings of Krumins et al. (2013), Brenner et al. (2016) and Gimenez (2018). Aerobic mineralization produced considerable amounts of DIC in line with previous work (Thamdrup & Canfield, 2000) while generating significantly less TA (Figure 3), leading to a low porewater pH. Denitrification and Fe reduction were less impactful on both DIC and TA production. With a high dTA/dR value (Table 3), TS oxidation with FeOx also contributed to alkalinity production. Consumption of TA was dominated by secondary redox reactions that oxidize reduced species with O_2. Due to fast kinetics, Fe^{2+} oxidation with O_2 and precipitation of FeS were the major TA consuming reactions. This contrasts with results of Brenner et al. (2016) who identified sulfide oxidation and nitrification as the dominant alkalinity consuming processes in the shallow water sediments in Southern North Sea. This discrepancy points to wide variability in sulfide oxidation kinetics reported by Krumins et al. (2013) which has a considerable impact on the net alkalinity generation due to sulfate reduction. Coupling of SO_4^{2-} reduction with FeS precipitation was shown to be an important mechanism for TA burial in shelves and with the lateral mixing it can provide a TA source in deeper Baltic Sea basins (Gustafsson et al., 2019). However, in our simulations, FeS formation was limited by Fe availability therefore, hydrogen sulfide accumulated in the porewater.

https://doi.org/10.5194/egusphere-2024-796
Preprint. Discussion started: 25 March 2024

Effect of carbonate mineral additions

After adding carbonate minerals, the concentration profiles of primary redox species largely remained unchanged (Figure 2). This is because the organic matter mineralization rate expressions (Table 3) do not contain dependencies on the carbonate system or pH, as is common in early diagenetic models (e.g., Rassmann et al., 2018; Jourabchi et al., 2008; Morse & Mackenzie, 1990). Mineral addition slightly decreased Fe^{2+} while increasing FeS concentrations. This is due to TA production due to carbonate dissolution, which elevates the pH and increases the saturation state of FeS (Table 3), promoting FeS formation.

The added carbonate minerals started to dissolve in our model, producing 1 DIC and 2 TA per carbon (Burdige et al., 2010; Zeebe & Wolf-Gladrow, 2001), so that both the pH and porewater saturation state increased (Cai et al., 2011). After 2 years, CO_2 production and lower pH in the oxic layer prevented full saturation, Ω was always above 0.9 and reached 1 at and below a depth of approximately 2.5 cm and subsequent decrease was observed below 12 cm. Buffering the surficial sediment is especially important as juvenile bivalves tend to reside in the shallower oxic layers (Green et al., 2009, 2013; Waldbusser et al., 2010). Following the addition of carbonates, the extent of the undersaturated conditions was constrained to the top 2 cm only while in the natural buffering scenario reported in Krumins et al. (2013), porewater remained undersaturated in the top 10 cm. This demonstrates the potential of OAE in mitigating surface sediment acidification and providing potential benefits for calcifiers living in the upper sediment layers. As mineral addition counteracts porewater acidification, it generates biogeochemical conditions conducive for the survival of juvenile bivalves.

https://doi.org/10.5194/egusphere-2024-796
Preprint. Discussion started: 25 March 2024

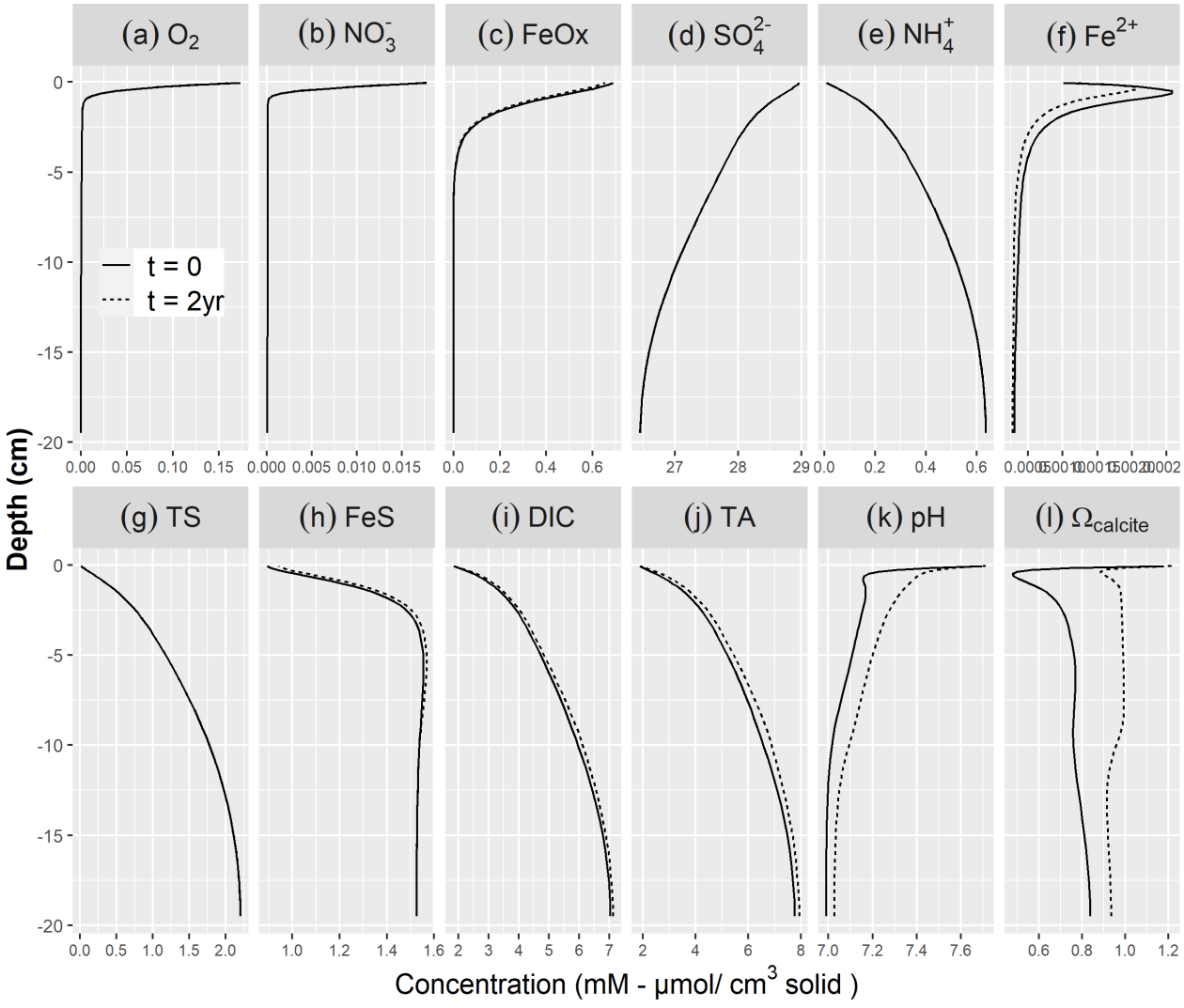

Figure 2. Simulated baseline porewater profiles of (a) O_2, (b) NO_3^-, (c) FeOx, (d) SO_4^{2-}, (e) NH_4^+, (f) Fe^{2+}, (g) TS, (h) FeS, (i) DIC, (j) TA, (k) pH and (l) $\Omega_{calcite}$. The solid lines denote the steady state profiles prior to the addition of calcite to the top 2 cm, while the dashed line indicate the simulated profiles 2 years after the mineral addition (some are coinciding with the solid lines and hence not visible). Dissolved constituents are in mmol/L porewater, while solids are given in µmol/cm^3 solid phase.

Our results were in line with literature showing that the main alkalinity producing processes were mineral dissolution, sulfate reduction, denitrification and sulfide oxidation with iron oxides (Krumins et al., 2013; Berelson et al., 2007). Although redox reactions generate alkalinity, they mostly have lower dTA/dDIC ratios and TA producing mineralization reactions are mostly coupled to TA consuming reoxidation reactions. Therefore, the net effect on TA production can be limited (Krumins et al.,

https://doi.org/10.5194/egusphere-2024-796
Preprint. Discussion started: 25 March 2024

2013). For example, the amount of TA generated by benthic denitrification was almost balanced out by NH_4^+ oxidation (Figure 3) which results in the small effect of N cycling on alkalinity. This is in line with previous studies showing strong coupling between oxidation/reduction of N in marine environment (Middelburg et al., 1996) and its weak impact on buffering capacity of the overlying water (Hu & Cai, 2011). However, because NH_4^+ is also produced by mineralization processes other than denitrification, the impact of N cycling on TA would change in environments where the importance of denitrification is different. Since reoxidation reactions are dependent on the availability of O_2, enhanced biological mixing can also increase TA consumption as previously demonstrated by Rao et al. (2014) for Fe^{2+} oxidation by O_2. Although total production of TA was around 1300 µmol cm^{-2} yr^{-1} (Figure 3, baseline with bio-calcite), total TA fluxes from bio-calcite were slightly lower, which points to the importance of consumption of TA in the oxic layer as observed in Figure 3 and previously reported in Krumins et al. (2013). Finally, before mineral addition, we observed a small production of calcite at the top of the sediment due to oversaturated conditions in overlying water. After the addition however, added mineral dissolved at depth which led to net dissolution and generation of alkalinity in the sediment column.

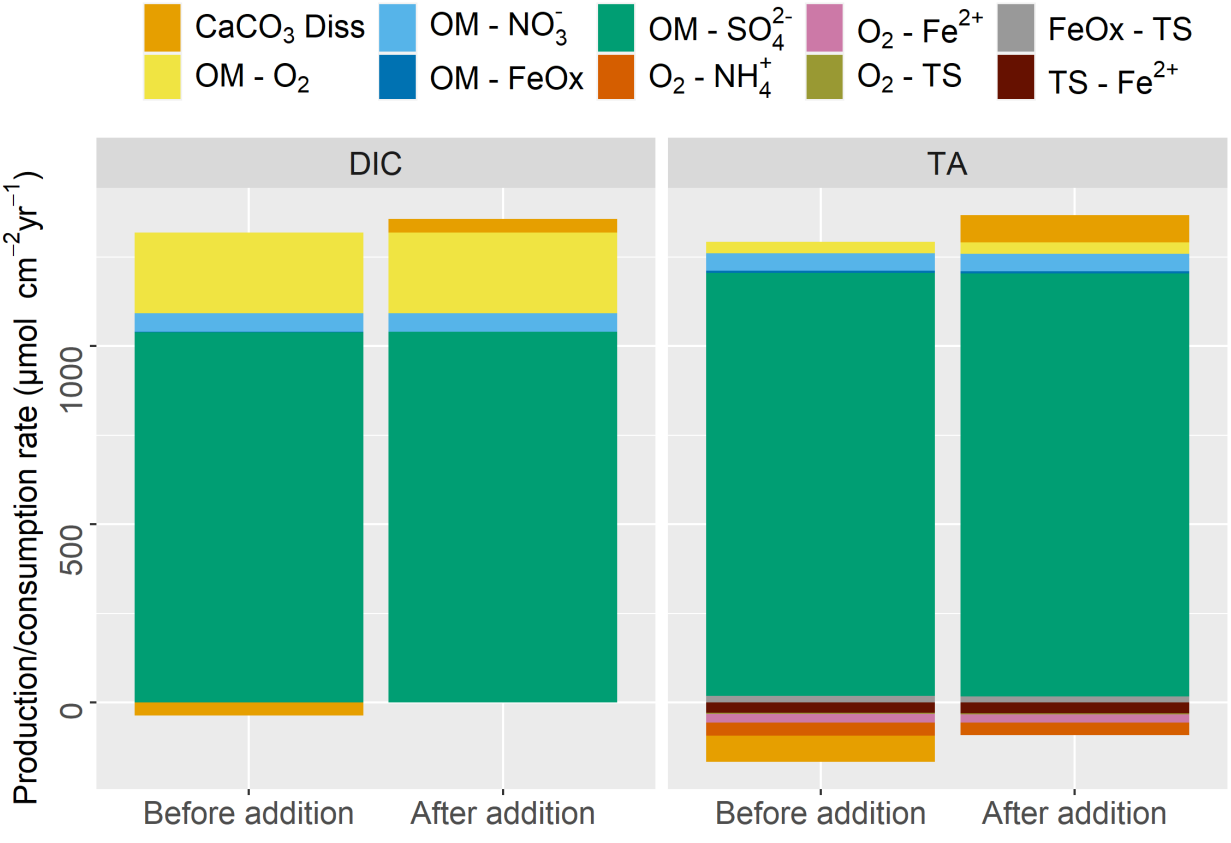

Figure 3. DIC and TA production (positive) and consumption (negative) by different early diagenetic processes integrated over the entire model domain for steady state (t = 0; before addition) and 2 years after the addition.

https://doi.org/10.5194/egusphere-2024-796
Preprint. Discussion started: 25 March 2024

Temporal evolution of buffering with different minerals and amounts

Longer-term simulations (50 yrs) were performed to investigate the evolution of the buffering with time, considering different amounts and types of minerals added. We focused on the biogeochemical conditions in the top 10 cm of sediment, because the surficial sediment is most relevant for juvenile bivalves impacted by ocean acidification. Depth-averaged TA concentrations in top 10 cm peaked around the 2nd year after addition, with a significant drop starting around year 10 for the 8% mineral addition and around year 15 for the 16% addition and then return to steady state levels after more than 30 years (Figure 4A). Doubling the amount of mineral added generated slightly higher TA and extended the length of the peak buffering period. The simulation of aragonite addition produced higher alkalinity concentrations than that of calcite by approximately 0.3 mM at the peak time reflecting its higher solubility. However, TA levels in aragonite application dropped faster after approximately 10 and 15 yrs and approached the initial pre-mineral application levels after about 30 and 40 years, for 8% and 16% additions, respectively. However, in calcite applications TA concentrations remained elevated until the end of the simulations (year 50).

https://doi.org/10.5194/egusphere-2024-796
Preprint. Discussion started: 25 March 2024

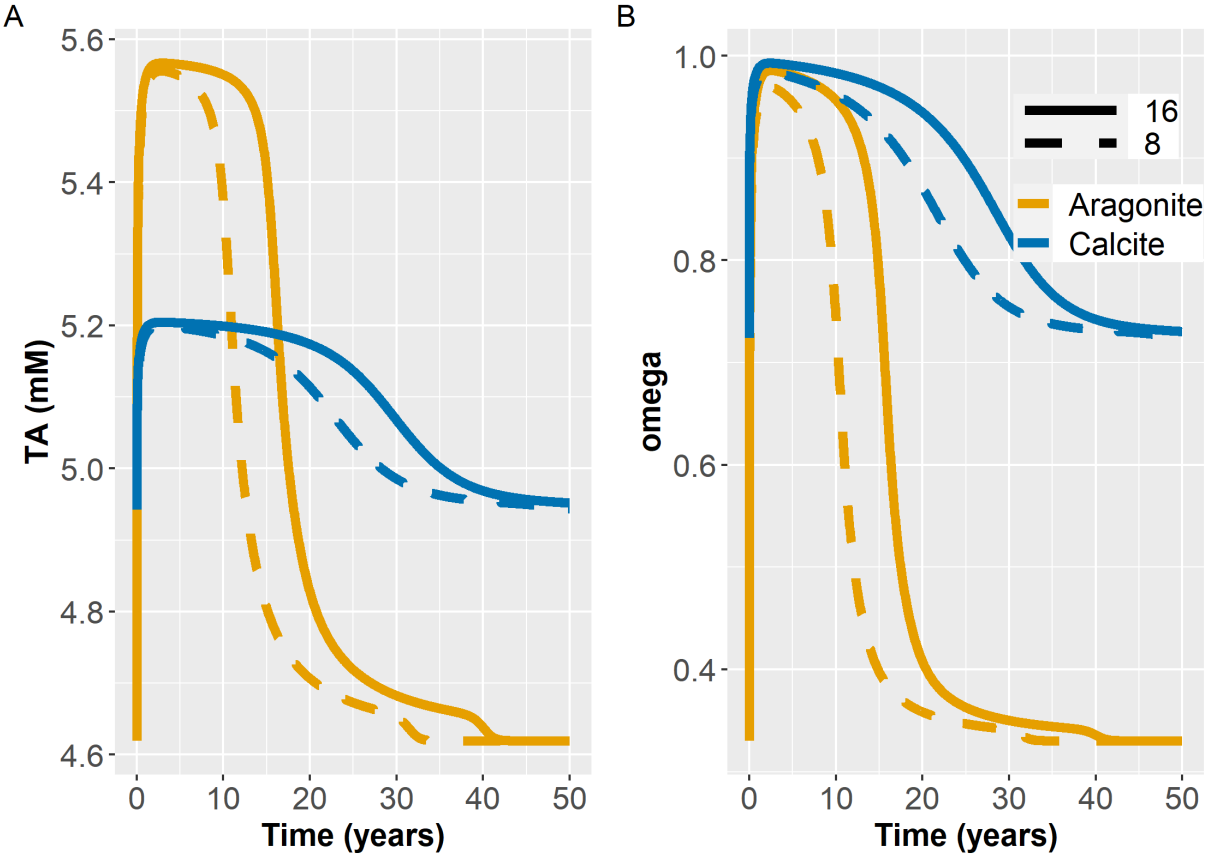

Figure 4. Temporal evolution of depth-averaged TA after addition of bio-aragonite and bio-calcite (A), and saturation states (B) in baseline simulation. Concentrations and saturation states are averaged over the top 10 cm of sediment. Colors show the type of mineral added. Solid and dashed lines show the addition of 16% and 8% respectively.

Being less stable than calcite, aragonite had a slightly faster dissolution rate constant and a larger solubility product (Burdige et al., 2010). Therefore, it generated higher TA concentrations and benthic fluxes early on. Because of its higher solubility, it initially took aragonite slightly longer to reach saturation than calcite. As the rate of dissolution is set to be proportional not only to the degree of undersaturation but also the carbonate mineral concentration (Eq. 2), doubling the mineral addition had a more pronounced effect for aragonite which was approaching saturation more slowly than calcite (Figure 4B). Burial of minerals led to a faster decrease in TA in aragonite due to its higher dissolution. Initial conditions in 50 years simulations with calcite had higher saturation state than aragonite implementation therefore, after the impact of addition got buried, calcite leveled at higher saturation state and TA than aragonite.

https://doi.org/10.5194/egusphere-2024-796
Preprint. Discussion started: 25 March 2024

Buffering response for different environments

The impact of mineral additions on the generation of alkalinity depends not only on the type of mineral added, but also on which early diagenetic processes dominate (Figure 3). The relative magnitude of these processes depends on a number of factors, including the rate of organic matter mineralization, the extent of bioturbation, the deposition fluxes of potential electron acceptors such as iron oxyhydroxides, and the composition of the overlying water. Varying these factors in our model, we explore their impact on both the conditions in the surficial sediment as well as the impact on benthic alkalinity fluxes.

In our simulations, mineral saturation states reached similar values at the end of the 2 years with low R_C^0 scenario generating the highest values (blue dots in Figure 5A). However, saturation was reached fastest in the deep bioturbation scenario which then decreased by years 1 and 2. Baseline, high FeOx flux and low R_C^0 scenarios showed a similar time course, while the addition of aragonite instead of calcite exhibited the slowest increase in saturation state. Depth-averaged TA concentrations were highest following the addition of aragonite. Deepening the bioturbation layer did not have much of an impact, the high FeOx flux scenario produced slightly lower TA than the baseline and the lowest amounts of alkalinity were produced by the low R_C^0 scenario. pH was buffered the most and increased the fastest in the aragonite implementation, followed by low R_C^0 conditions. Although the deep mixed layer scenario increased pH faster than baseline and high FeOx flux scenario, these three scenarios converged to a similar pH as buffering developed. The highest benthic TA fluxes were generated during the dissolution of aragonite while the lowest values were produced in the low R_C^0 scenario. Baseline and deeper bioturbation layer scenarios produced very similar results while high FeOx flux scenario produced slightly lower TA fluxes. Lowering overlying water pH led to decreases in saturation state and pH while increasing concentration and flux of alkalinity.

https://doi.org/10.5194/egusphere-2024-796
Preprint. Discussion started: 25 March 2024

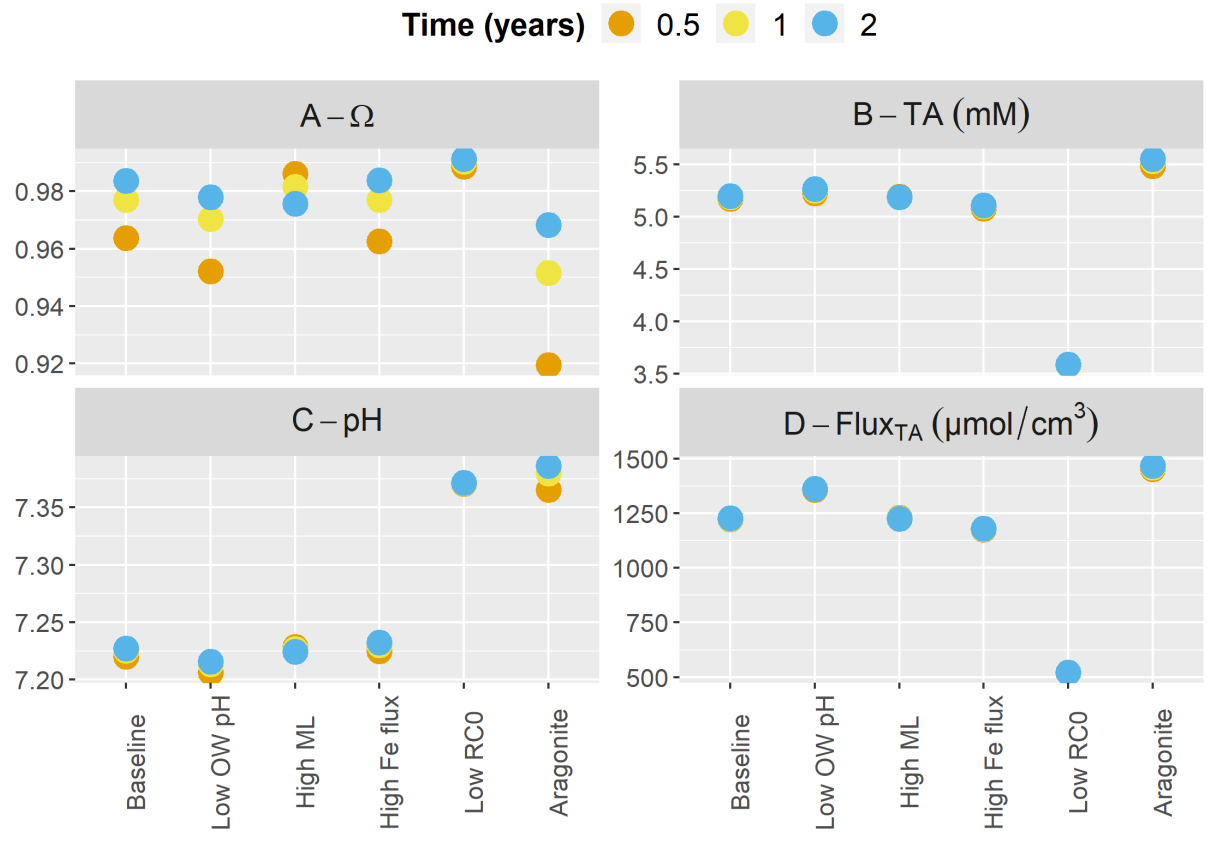

Figure 5. Buffering response 2 years after carbonate mineral additions for a range of environmental conditions. Concentrations are averaged over top 10cm. Scenarios listed on x axis (from left to right): baseline simulation with calcite; baseline with lower overlying water pH (7.8); baseline with deeper mixed layer (10 cm); baseline with higher Fe flux (10 µmol cm^{-2} yr^{1}); baseline with lower R_C^0 (200 µmol cm^{-3}); baseline with aragonite instead of calcite.

Due to the higher solubility and hence larger degree of undersaturation, initial aragonite dissolution was faster than calcite. Hence, aragonite produced the largest TA in 2 years, generated highest benthic TA fluxes, and increased the pH the most. The addition of aragonite produced more buffering than the scenario with lower OM mineralization which shows the potential of artificial buffering overcoming the acidification impact due to OM mineralization.

Increased FeOx input to the sediment led to enhanced FeOx reduction which produced TA. However, increased reoxidation of Fe^{2+} led to decreased availability of O_2 and consumption of TA. This balanced out the additional TA produced through FeOx reduction and led to an additional net consumption of ~46 µmol cm^{-2} yr^{-1} of TA. Overall, increased iron oxide supply led to slight decreases in TA concentrations and fluxes showing an effect similar to decrease in OM mineralization rate in a smaller magnitude as also seen with small increases in pH (Figure 5).

https://doi.org/10.5194/egusphere-2024-796
Preprint. Discussion started: 25 March 2024

Deeper bioturbation led to faster downward mixing and subsequent dissolution of the added mineral which then led to rapid increase in TA, pH and saturation state. Higher mixing led to faster transport of minerals inducing enhanced dissolution in year 0.5 (i.e., Figure 5, higher buffering 0.5 than 2 years after mineral addition). However, faster transport extended the depth of buffering and diluted dissolution products, which caused a slight decrease in pH and saturation state after 2 years at the top 10 cm (Figure 5).

A lower pH in the overlying water led to a lower pH in the porewater and less saturated conditions in surface sediments (Figure 5). This promoted mineral dissolution and therefore led to increased TA production and flux to the overlying water. This demonstrates the sensitivity of buffering towards the overlying water conditions.

TA production and flux was significantly lower in low OM reaction rate scenario (Figure 5D) which showed the critical impact of OM mineralization on TA dynamics. The lower rate of OM mineralization decreases TA production, both through the reduction of overall mineralization rates, and the reduction of the relative contribution of anaerobic mineralization pathways like dissimilatory sulfate reduction. The low rate of mineralization also led to reduced H^+ production, which in turn slows carbonate dissolution (Morse & MacKenzie, 1990). However, even with lower dissolution, this situation led to higher pH than the baseline suggesting that the artificial buffering might not be needed to maintain saturated conditions in environments where OM reactivity is low. On the other hand, especially in deeper layers where the surficial mineral addition is not as effective, TA and mineral saturation states will be lower due to lower anaerobic TA production. Notably, the effect of changing the OM mineralization rate is not linear, and halving the rate reduced the benthic alkalinity flux by a factor of about 2.5. Aside from the (minor) impact on the partitioning of OM mineralization between metabolic pathways, this mainly reflects that changes in mineralization rates lead to differences in the porewater conditions, which in turn alter the rate of mineral dissolution.

Our model demonstrates the potential for coastal sediment alkalinization to improve the biogeochemical conditions for juvenile calcifying organisms living in surficial sediments. However, alkalinity fluxes are highly sensitive to overlying water conditions, temporal changes in overlying water should be considered. These changes include diel patterns in photosynthesis and respiration impacting benthic fluxes (Cyronak et al., 2013b; Yamamato et al., 2015), seasonal changes such as temperature (Rao et al., 2014) and long-term changes such as anthropogenic impact (Pacella et al., 2018). In addition, in particular in near-shore shallow water environments, one may have to take into consideration the input of groundwater (Cyronak et al., 2013a), advective flow through sand ripples (Huettel et al., 1998) and other factors driving advective flow in marine sediments (Santos et al., 2012), which can impact sediment biogeochemistry and alkalinity fluxes. Furthermore, the prediction of the time course of buffering by mineral dissolution may need to consider dissolution rate expressions that account for changes in mineral surface areas, rather than bulk concentrations (Morse et al., 2007), and the potential for loosing minerals deposited to the sediment in high-energy environments.

https://doi.org/10.5194/egusphere-2024-796
Preprint. Discussion started: 25 March 2024

3.3. Potential impact of benthic fluxes on marine CO_2 uptake

Benthic alkalinity fluxes are critical for water column C dynamics especially in shallow water environments where water column and atmospheric interactions are more sensitive to processes occurring in the sediment (Brenner et al., 2016). The significant decrease in shells due to overharvesting has likely altered alkalinity cycling in estuarine waters, such as Chesapeake Bay (Waldbusser et al., 2013). One outcome of this benthic-pelagic connection is the impact of benthic fluxes on oceanic CO_2 uptake which was estimated to have significant influence in the North Sea (Thomas et al., 2009), and the potential for shallow water sediment alkalinization to alter overlying water.

We estimated the potential impact of enhanced sediment TA fluxes on atmospheric CO_2 uptake in Yaquina Bay, OR (USA) using the diagenetic model output in a simple box model. The bay was found to be net heterotrophic, with tidal exchange and net respiration in the water column impacting air-sea CO_2 flux in the bay most. The impact of sediment buffering on the air-sea CO_2 was estimated as the difference in atmospheric CO_2 fluxes between before and after the mineral addition. Mineral addition resulted in a TA flux enhancement of ~126 μmol cm^{-2} yr^{-1} and an increase of CO_2 uptake by approximately 58 μmol cm^{-2} yr^{-1}, which was comparable to previous studies (Brenner et al., 2016). Scaling to a 10 m water depth (or per liter of water), this stoichiometrically estimated marine carbon dioxide removal (mCDR) due to the application and subsequent dissolution of carbonate minerals by the sediments results in a similar amount of mCDR as the current estimates of the anthropogenic C (C_{anth}) concentration in the US Pacific coast waters, 30-60 μmol L^{-1} (Feely et al. 2016, Pacella et al. 2024). It is important to note three key points in this estimate: (1) the uptake of C_{anth} by marine waters from anthropogenic activities results in an increase of DIC without any concurrent change in alkalinity, thus acidification. (2) alkalinity enhancement shifts the carbonate speciation and allows increased uptake of atmospheric CO_2 by marine waters. Thus, ocean alkalinity enhancement increases the total amount of C_{anth} in seawater. However, while C_{anth} and DIC both increase with OAE, (3) the mineral dissolution due to sediment buffering results in an increase in the Alk:DIC, thus providing the mCDR benefit of atmospheric removal as well as mitigating existing acidification impacts. The mCDR effect here, while notable, is however miniscule compared to the total air-sea exchange flux, which is driven by in tidal exchange of DIC and alkalinity between the bay and the coastal ocean. The signal to noise of this potentially significant effect also highlights the existing measurement challenges in accurately discerning OAE effects within coastal systems.

4. Conclusions

Our study successfully combines lab experiments and modeling to investigate the impact of coastal alkalinity enhancement, points to critical aspects to be considered and presents the potential of carbonate additions as a mitigation strategy for the effects of climate change in coastal settings. We demonstrated that addition of minerals increased pH and saturation state of the sediment over the timespan of a few months and had the potential to persist over 30-40 years. During the peak buffering period, porewater in the top 10 cm of the sediment was almost fully saturated with respect to the mineral added, which implies favorable conditions for benthic calcifying organisms. We showed that two main pathways of producing TA in the sediment were sulfate reduction and mineral dissolution. We also demonstrated that the type of mineral was an important

https://doi.org/10.5194/egusphere-2024-796
Preprint. Discussion started: 25 March 2024

factor in quantifying benthic fluxes and that the application of an increased amount of minerals was effective in extending the duration rather than the strength of the buffering.

Our analysis suggests that buffering through mineral additions to coastal sediments can establish biogeochemical conditions that are conducive for the growth and development of calcifying benthic organisms. However, the effect of mineral additions can vary substantially between environments. Sensitivity analyses demonstrated that the OM mineralization had a significant impact on mineral dissolution, pH and mineral saturation. The type of mineral added also showed significant effect with aragonite producing more TA and higher pH. Increased mixing depth led to a faster increase in saturation state while increased iron flux caused reduction in TA concentration and benthic fluxes. Overall, the addition of minerals with faster dissolution rates would be most effective especially in environments with high OM degradation and undersaturated water conditions. Similarly, the type of mineral and the environmental conditions affect marine CDR potential through benthic fluxes.

Ocean acidification research gained popularity in the past decade, but with its complicated effects on ocean life and biogeochemistry through a range of biogeochemical processes, it still is challenging to predict its overall impacts in the ocean (Riebesell and Gattuso, 2015; Middelburg et al., 2020). In coastal systems, $CaCO_3$ can act as a natural buffer. Combined with other anthropogenic impacts (i.e., eutrophication, Cai et al., 2011; Egleston et al., 2010) the impact of ocean acidification would be enhanced and therefore require interventions to sustain ecosystem health (Waldbusser et al., 2015). However, large-scale geoengineering methods such as OAE can have large uncertainties with regard to side effects and implementation (Caldeira et al., 2013). These side effects can include unforeseen ecological feedback such as changes in species composition (Bach et al., 2019; Köhler et al., 2013) and the potential rapid changes after OAE implementations (González et al., 2018). Therefore, studies should combine field, lab and modeling components (Meysman & Montserrat, 2017) to improve predictive capabilities and decrease uncertainty.

Code Availability

The reaction transport model can be found at: https://bitbucket.org/MeileLab/kadir_oa/src/master/

Data Availability

Data for this manuscript is available in Myers (2022).

Author contribution

Lab experiments were designed by GW and TM, carried out by TM with the guidance of GW. KB developed the numerical model with guidance of CM and carried out the simulations. KB prepared the initial draft of the manuscript with significant input from CM, TM and GW.

Competing interests

The authors declare that they have no conflict of interest.

Acknowledgements

The authors would like to thank the ClimateWorks Foundation for funding and Jurjen Rooze for input on the model implementation.

https://doi.org/10.5194/egusphere-2024-796
Preprint. Discussion started: 25 March 2024

References

Aller, R. C. (1982). The effects of macrobenthos on chemical properties of marine sediment and overlying water. In Animal-sediment relations: the biogenic alteration of sediments (pp. 53-102). Boston, MA: Springer US.

Andersson, A. J., Mackenzie, F. T., & Lerman, A. (2005). Coastal ocean and carbonate systems in the high CO2 world of the Anthropocene. American Journal of Science, 305(9), 875-918.

D'Andrea, A. F., & DeWitt, T. H. (2009). Geochemical ecosystem engineering by the mud shrimp Upogebia pugettensis (Crustacea: Thalassinidae) in Yaquina Bay, Oregon: Density-dependent effects on organic matter remineralization and nutrient cycling. Limnology and Oceanography, 54(6), 1911-1932.

Bach, L. T., Gill, S. J., Rickaby, R. E., Gore, S., & Renforth, P. (2019). CO_2 removal with enhanced weathering and ocean alkalinity enhancement: potential risks and co-benefits for marine pelagic ecosystems. Frontiers in Climate, 1, 7.

Bandstra, L., Hales, B., & Takahashi, T. (2006). High-frequency measurements of total CO2: Method development and first oceanographic observations. Marine Chemistry, 100(1-2), 24-38.

Barton, A., Hales, B., Waldbusser, G. G., Langdon, C., & Feely, R. A. (2012). The Pacific oyster, Crassostrea gigas, shows negative correlation to naturally elevated carbon dioxide levels: Implications for near-term ocean acidification effects. Limnology and oceanography, 57(3), 698-710.

Barton, A., Waldbusser, G. G., Feely, R. A., Weisberg, S. B., Newton, J. A., Hales, B., ... & McLaughlin, K. (2015). Impacts of coastal acidification on the Pacific Northwest shellfish industry and adaptation strategies implemented in response. *Oceanography*, *28*(2), 146-159.

Berelson, W. M., Balch, W. M., Najjar, R., Feely, R. A., Sabine, C., & Lee, K. (2007). Relating estimates of $CaCO_3$ production, export, and dissolution in the water column to measurements of $CaCO_3$ rain into sediment traps and dissolution on the sea floor: A revised global carbonate budget. Global Biogeochemical Cycles, 21(1).

Berner, R. A. (1980). Early diagenesis: a theoretical approach. 241 p. Princeton University Press.

Boudreau, B. P. (1984). On the equivalence of nonlocal and radial-diffusion models for porewater irrigation. Journal of Marine Research, 42(3), 731-735.

Boudreau, B. P. (1996). The diffusive tortuosity of fine-grained unlithified sediments. Geochimica et Cosmochimica Acta, 60(16), 3139-3142.

Boudreau, B. P. (1997). Diagenetic models and their implementation. 414 p. (Vol. 505). Berlin: Springer.

Brenner, H., Braeckman, U., Le Guitton, M., & Meysman, F. J. (2016). The impact of sedimentary alkalinity release on the water column CO_2 system in the North Sea. Biogeosciences, 13(3), 841-863.

Burdige, D. J. (2007). Preservation of organic matter in marine sediments: controls, mechanisms, and an imbalance in sediment organic carbon budgets? Chemical Reviews, 107(2), 467-485.

Burdige, D. J., Hu, X., & Zimmerman, R. C. (2010). The widespread occurrence of coupled carbonate dissolution/reprecipitation in surface sediments on the Bahamas Bank. American Journal of Science, 310(6), 492-521.

https://doi.org/10.5194/egusphere-2024-796
Preprint. Discussion started: 25 March 2024

Cai, W. J., Hu, X., Huang, W. J., Murrell, M. C., Lehrter, J. C., Lohrenz, S. E., ... & Gong, G. C. (2011). Acidification of subsurface coastal waters enhanced by eutrophication. Nature geoscience, 4(11), 766-770.

Cai, W. J., Huang, W. J., Luther III, G. W., Pierrot, D., Li, M., Testa, J., ... & Kemp, W. M. (2017). Redox reactions and weak buffering capacity lead to acidification in the Chesapeake Bay. Nature Communications, 8(1), 369.

Caldeira, K., Bala, G., & Cao, L. (2013). The science of geoengineering. Annual Review of Earth and Planetary Sciences, 41, 231-256.

Cyronak, T., Santos, I. R., Erler, D. V., & Eyre, B. D. (2013a). Groundwater and porewater as major sources of alkalinity to a fringing coral reef lagoon (Muri Lagoon, Cook Islands). Biogeosciences, 10(4), 2467-2480.

Cyronak, T., Santos, I. R., McMahon, A., & Eyre, B. D. (2013b). Carbon cycling hysteresis in permeable carbonate sands over a diel cycle: Implications for ocean acidification. Limnology and Oceanography, 58(1), 131-143.

Dickson, A. G. (1981). An exact definition of total alkalinity and a procedure for the estimation of alkalinity and total inorganic carbon from titration data. Deep Sea Research Part A. Oceanographic Research Papers, 28(6), 609-623.

Doney, S. C., Fabry, V. J., Feely, R. A., & Kleypas, J. A. (2009). Ocean acidification: the other CO_2 problem. Annual Review of Marine Science, 1, 169-192.

Edmond, J. M., & Gieskes, J. M. T. M. (1970). On the calculation of the degree of saturation of sea water with respect to calcium carbonate under in situ conditions. Geochimica et cosmochimica acta, 34(12), 1261-1291.

Egleston, E. S., Sabine, C. L., & Morel, F. M. (2010). Revelle revisited: Buffer factors that quantify the response of ocean chemistry to changes in DIC and alkalinity. Global Biogeochemical Cycles, 24(1).

Ekstrom, J. A., Suatoni, L., Cooley, S. R., Pendleton, L. H., Waldbusser, G. G., Cinner, J. E., ... & Portela, R. (2015). Vulnerability and adaptation of US shellfisheries to ocean acidification. Nature Climate Change, 5(3), 207-214.

Fabry, V. J., Seibel, B. A., Feely, R. A., & Orr, J. C. (2008). Impacts of ocean acidification on marine fauna and ecosystem processes. ICES Journal of Marine Science, 65(3), 414-432.

Feely, R. A., Alin, S. R., Carter, B., Bednaršek, N., Hales, B., Chan, F., ... & Juranek, L. (2016). Chemical and biological impacts of ocean acidification along the west coast of North America. Estuarine, Coastal and Shelf Science, 183, 260-270.

Fry, C. H., Tyrrell, T., Hain, M. P., Bates, N. R., & Achterberg, E. P. (2015). Analysis of global surface ocean alkalinity to determine controlling processes. Marine Chemistry, 174, 46-57.

Gimenez, I., Waldbusser, G. G., & Hales, B. (2018). Ocean acidification stress index for shellfish (OASIS): Linking Pacific oyster larval survival and exposure to variable carbonate chemistry regimes. Elem Sci Anth, 6, 51.

Goldenberg, S. U., Riebesell, U., Brüggemann, D., Börner, G., Sswat, M., Folkvord, A., ... & Moyano, M. (2024). Viability of coastal fish larvae under ocean alkalinity enhancement: from organisms to communities. EGUsphere.

González, M. F., Ilyina, T., Sonntag, S., & Schmidt, H. (2018). Enhanced Rates of Regional Warming and Ocean Acidification After Termination of Large-Scale Ocean Alkalinization. Geophysical Research Letters, 45(14), 7120-7129.

Green, M. A., Waldbusser, G. G., Hubazc, L., Cathcart, E., & Hall, J. (2013). Carbonate mineral saturation state as the recruitment cue for settling bivalves in marine muds. Estuaries and Coasts, 36, 18-27.

https://doi.org/10.5194/egusphere-2024-796
Preprint. Discussion started: 25 March 2024

Green, M. A., Waldbusser, G. G., Reilly, S. L., Emerson, K., & O'Donnell, S. (2009). Death by dissolution: sediment saturation state as a mortality factor for juvenile bivalves. Limnology and Oceanography, 54(4), 1037-1047.

Gustafsson, E., Hagens, M., Sun, X., Reed, D. C., Humborg, C., Slomp, C. P., & Gustafsson, B. G. (2019). Sedimentary alkalinity generation and long-term alkalinity development in the Baltic Sea. Biogeosciences, 16(2), 437-456.

Hales, B., Suhrbier, A., Waldbusser, G. G., Feely, R. A., & Newton, J. A. (2017). The carbonate chemistry of the "fattening line," Willapa Bay, 2011–2014. Estuaries and Coasts, 40, 173-186.

Hales, B., Takahashi, T., & Bandstra, L. (2005). Atmospheric CO_2 uptake by a coastal upwelling system. Global Biogeochemical Cycles, 19(1).

Hangx, S. J., & Spiers, C. J. (2009). Coastal spreading of olivine to control atmospheric CO_2 concentrations: A critical analysis of viability. International Journal of Greenhouse Gas Control, 3(6), 757-767.

Hartmann, J., West, A. J., Renforth, P., Köhler, P., De La Rocha, C. L., Wolf-Gladrow, D. A., ... & Scheffran, J. (2013). Enhanced chemical weathering as a geoengineering strategy to reduce atmospheric carbon dioxide, supply nutrients, and mitigate ocean acidification. Reviews of Geophysics, 51(2), 113-149.

Hofmann, G. E., Smith, J. E., Johnson, K. S., Send, U., Levin, L. A., Micheli, F., ... & Martz, T. R. (2011). High-frequency dynamics of ocean pH: a multi-ecosystem comparison. PloS One, 6(12), e28983.

Hofmann, A. F., Soetaert, K., Middelburg, J. J., & Meysman, F. J. (2010). AquaEnv: An Aquatic Acid–Base Modelling Environment in R. Aquatic Geochemistry, 16, 507-546.

Hu, X., & Cai, W. J. (2011). The impact of denitrification on the atmospheric CO_2 uptake potential of seawater. Marine Chemistry, 127(1-4), 192-198.

Huettel, M., Ziebis, W., Forster, S., & Luther Iii, G. W. (1998). Advective transport affecting metal and nutrient distributions and interfacial fluxes in permeable sediments. Geochimica et Cosmochimica Acta, 62(4), 613-631.

Jahnke, R. A., Craven, D. B., & Gaillard, J. F. (1994). The influence of organic matter diagenesis on $CaCO_3$ dissolution at the deep-sea floor. Geochimica et Cosmochimica Acta, 58(13), 2799-2809.

Jourabchi, P., Meile, C., Pasion, L. R., & Van Cappellen, P. (2008). Quantitative interpretation of pore water O_2 and pH distributions in deep-sea sediments. Geochimica et Cosmochimica Acta, 72(5), 1350-1364.

Jourabchi, P., Van Cappellen, P., & Regnier, P. (2005). Quantitative interpretation of pH distributions in aquatic sediments: A reaction-transport modeling approach. American Journal of Science, 305(9), 919-956.

Köhler, P., Abrams, J. F., Völker, C., Hauck, J., & Wolf-Gladrow, D. A. (2013). Geoengineering impact of open ocean dissolution of olivine on atmospheric CO_2, surface ocean pH and marine biology. Environmental Research Letters, 8(1), 014009.

Krumins, V., Gehlen, M., Arndt, S., Van Cappellen, P., & Regnier, P. (2013). Dissolved inorganic carbon and alkalinity fluxes from coastal marine sediments: model estimates for different shelf environments and sensitivity to global change. Biogeosciences, 10(1), 371-398.

https://doi.org/10.5194/egusphere-2024-796
Preprint. Discussion started: 25 March 2024

Luff, R., & Wallmann, K. (2003). Fluid flow, methane fluxes, carbonate precipitation and biogeochemical turnover in gas hydrate-bearing sediments at Hydrate Ridge, Cascadia Margin: numerical modeling and mass balances. Geochimica et Cosmochimica Acta, 67(18), 3403-3421.

Meile, C., & Cappellen, P. V. (2003). Global estimates of enhanced solute transport in marine sediments. Limnology and Oceanography, 48(2), 777-786.

Meysman, F. J., & Montserrat, F. (2017). Negative CO2 emissions via enhanced silicate weathering in coastal environments. Biology Letters, 13(4), 20160905.

Middelburg, J. J., Soetaert, K., & Herman, P. M. (1997). Empirical relationships for use in global diagenetic models. Deep Sea Research Part I: Oceanographic Research Papers, 44(2), 327-344.

Middelburg, J. J., Soetaert, K., Herman, P. M., & Heip, C. H. (1996). Denitrification in marine sediments: A model study. Global Biogeochemical Cycles, 10(4), 661-673.

Middelburg, J. J., Soetaert, K., & Hagens, M. (2020). Ocean alkalinity, buffering and biogeochemical processes. Reviews of Geophysics, 58(3), e2019RG000681.

Millero, F. J. (2010). Carbonate constants for estuarine waters. Marine and Freshwater Research, 61(2), 139-142.

Montserrat, F., Renforth, P., Hartmann, J., Leermakers, M., Knops, P., & Meysman, F. J. (2017). Olivine dissolution in seawater: implications for CO_2 sequestration through enhanced weathering in coastal environments. Environmental Science & Technology, 51(7), 3960-3972.

Morse, J. W., Arvidson, R. S., & Lüttge, A. (2007). Calcium carbonate formation and dissolution. Chemical Reviews, 107(2), 342-381.

Morse, J. W., & Mackenzie, F. T. (1990). Geochemistry of sedimentary carbonates. Elsevier.

Mucci, A. (1983). The solubility of calcite and aragonite in seawater at various salinities, temperatures, and one atmosphere total pressure. American Journal of Science, 283(7), 780-799.

Mucci, A., Sundby, B., Gehlen, M., Arakaki, T., Zhong, S., & Silverberg, N. (2000). The fate of carbon in continental shelf sediments of eastern Canada: a case study. Deep Sea Research Part II: Topical Studies in Oceanography, 47(3-4), 733-760.

Myers, T. J. (2022). Buffering Estuarine Sediments Against Acidification. Master's Thesis. 77p. Oregon State University. https://ir.library.oregonstate.edu/concern/graduate_thesis_or_dissertations/br86bb964

Pacella, S. R., Brown, C. A., Labiosa, R. G., Hales, B., Mochon Collura, T. C., Evans, W., & Waldbusser, G. G. (2024). Feedbacks between estuarine metabolism and anthropogenic CO_2 accelerate local rates of ocean acidification and hasten threshold exceedances. Journal of Geophysical Research: Oceans, 129(3), e2023JC020313.

Pacella, S. R., Brown, C. A., Waldbusser, G. G., Labiosa, R. G., & Hales, B. (2018). Seagrass habitat metabolism increases short-term extremes and long-term offset of CO_2 under future ocean acidification. Proceedings of the National Academy of Sciences, 115(15), 3870-3875.

Paul, A. J., Haunost, M., Goldenberg, S. U., Hartmann, J., Sanchez, N. S., Schneider, J., ... & Riebesell, U. (2024). Ocean alkalinity enhancement in an open ocean ecosystem: Biogeochemical responses and carbon storage durability. EGUsphere.

https://doi.org/10.5194/egusphere-2024-796
Preprint. Discussion started: 25 March 2024

Rao, A. M., Malkin, S. Y., Montserrat, F., & Meysman, F. J. (2014). Alkalinity production in intertidal sands intensified by lugworm bioirrigation. Estuarine, Coastal and Shelf Science, 148, 36-47.

Rassmann, J., Lansard, B., Pozzato, L., & Rabouille, C. (2016). Carbonate chemistry in sediment porewaters of the Rhône River delta driven by early diagenesis (northwestern Mediterranean). Biogeosciences, 13(18), 5379-5394.

Rassmann, J., Lansard, B., Gazeau, F., Guidi-Guilvard, L., Pozzato, L., Alliouane, S., ... & Rabouille, C. (2018). Impact of ocean acidification on the biogeochemistry and meiofaunal assemblage of carbonate-rich sediments: Results from core incubations (Bay of Villefranche, NW Mediterranean Sea). Marine Chemistry, 203, 102-119.

Renforth, P., & Henderson, G. (2017). Assessing ocean alkalinity for carbon sequestration. Reviews of Geophysics, 55(3), 636-674.

Riebesell, U., & Gattuso, J. P. (2015). Lessons learned from ocean acidification research. Nature Climate Change, 5(1), 12-14.

Rooze, J., Egger, M., Tsandev, I., & Slomp, C. P. (2016). Iron-dependent anaerobic oxidation of methane in coastal surface sediments: Potential controls and impact. Limnology and Oceanography, 61(S1), S267-S282.

Rooze, J., Peterson, L., Peterson, R. N., & Meile, C. (2020). Porewater flow patterns in surficial cold seep sediments inferred from conservative tracer profiles and early diagenetic modeling. Chemical Geology, 536, 119468.

Santos, I. R., Eyre, B. D., & Huettel, M. (2012). The driving forces of porewater and groundwater flow in permeable coastal sediments: A review. Estuarine, Coastal and Shelf Science, 98, 1-15.

Soetaert, K., Hofmann, A. F., Middelburg, J. J., Meysman, F. J., & Greenwood, J. (2007). The effect of biogeochemical processes on pH. Marine Chemistry, 106(1-2), 380-401.

Soetaert, K., Petzoldt, T., & Meysman, F. (2010). Marelac: Tools for aquatic sciences. https://cran.r-project.org/package=marelac

Su, J., Cai, W. J., Brodeur, J., Chen, B., Hussain, N., Yao, Y., ... & Kemp, W. M. (2020). Chesapeake Bay acidification buffered by spatially decoupled carbonate mineral cycling. Nature Geoscience, 13(6), 441-447.

Taylor, L. L., Quirk, J., Thorley, R. M., Kharecha, P. A., Hansen, J., Ridgwell, A., ... & Beerling, D. J. (2016). Enhanced weathering strategies for stabilizing climate and averting ocean acidification. Nature Climate Change, 6(4), 402-406.

Thamdrup, B., & Canfield, D. E. (2000). Benthic respiration in aquatic sediments. In Methods in ecosystem science (pp. 86-103). New York, NY: Springer New York.

Thomas, H., Schiettecatte, L. S., Suykens, K. O. N. E., Koné, Y. J. M., Shadwick, E. H., Prowe, A. F., ... & Borges, A. V. (2009). Enhanced ocean carbon storage from anaerobic alkalinity generation in coastal sediments. Biogeosciences, 6(2), 267-274.

Thullner, M., Dale, A. W., & Regnier, P. (2009). Global-scale quantification of mineralization pathways in marine sediments: A reaction-transport modeling approach. Geochemistry, geophysics, geosystems, 10(10).

Waldbusser, G. G., Bergschneider, H., & Green, M. A. (2010). Size-dependent pH effect on calcification in post-larval hard clam Mercenaria spp. Marine Ecology Progress Series, 417, 171-182.

https://doi.org/10.5194/egusphere-2024-796
Preprint. Discussion started: 25 March 2024

Waldbusser, G. G., Hales, B., Langdon, C. J., Haley, B. A., Schrader, P., Brunner, E. L., ... & Gimenez, I. (2015). Saturation-state sensitivity of marine bivalve larvae to ocean acidification. Nature Climate Change, 5(3), 273-280.

Waldbusser, G. G., Powell, E. N., & Mann, R. (2013). Ecosystem effects of shell aggregations and cycling in coastal waters: an example of Chesapeake Bay oyster reefs. Ecology, 94(4), 895-903.

Waldbusser, G. G., & Salisbury, J. E. (2014). Ocean acidification in the coastal zone from an organism's perspective: multiple system parameters, frequency domains, and habitats. Annual Review of Marine Science, 6, 221-247.

Waldbusser, G. G., Steenson, R. A., & Green, M. A. (2011). Oyster shell dissolution rates in estuarine waters: effects of pH and shell legacy. Journal of Shellfish Research, 30(3), 659-669.

Wang, Y., & Van Cappellen, P. (1996). A multicomponent reactive transport model of early diagenesis: Application to redox cycling in coastal marine sediments. Geochimica et Cosmochimica Acta, 60(16), 2993-3014.

Wolf-Gladrow D.A., Zeeber, R.E., Klaas, C., Koertzinger, A. and Dickson, A.G. (2007). Total alkalinity: The explicit conservative expression and its application to biogeochemical processes. Marine Chemistry, 106, 287-300.

Yamamoto, S., Kayanne, H., Tokoro, T., Kuwae, T., & Watanabe, A. (2015). Total alkalinity flux in coral reefs estimated from eddy covariance and sediment pore-water profiles. Limnology and Oceanography, 60(1), 229-241.

Zeebe, R. E., & Wolf-Gladrow, D. (2001). CO_2 in seawater: equilibrium, kinetics, isotopes (No. 65). Gulf Professional Publishing.

Zwarts, L., & Wanink, J. (1989). Siphon size and burying depth in deposit-and suspension-feeding benthic bivalves. Marine Biology, 100, 227-240.